# EXPERIMENTAL OBSERVATION OF NON-IDEAL NOZZLE FLOW OF SILOXANE VAPOR MDM

Andrea Spinelli[1*], Alberto Guardone[2], Fabio Cozzi[1], Margherita Carmine[1], Renata Cheli[1], Marta Zocca[2], Paolo Gaetani[1], Vincenzo Dossena[1]

[1] Politecnico di Milano, Department of Energy
Via Lambruschini 4, 20156 Milano, Italy
e-mail: andrea.spinelli@polimi.it

[2] Politecnico di Milano, Department of Aerospace Science and Technology
Via La Masa 34, 20156 Milano, Italy
e-mail: alberto.guardone@polimi.it

* Corresponding Author

## ABSTRACT

The first experimental results from the Test-Rig for Organic Vapors (TROVA) at Politecnico di Milano are reported. The facility implements an Organic Rankine Cycle (ORC) where the expansion process takes place within a straight axis convergent-divergent nozzle, which is the simplest geometry representative of an ORC turbine blade passage. In order to reduce the required input thermal power, a batch operating mode was selected for the plant. Experimental runs with air allowed to verify the throttling valve operation and the measurement techniques, which include total pressure and temperature measurements in the settling chamber, static pressure measurements along the nozzle axis. A double-passage Schlieren technique is used to visualize the flow field in the nozzle throat and divergent section and to determine the position of shock waves within the flow field. The first experimental observation of non-ideal nozzle flows are presented for the expansion of siloxane fluid MDM ($C_8H_{24}O_2Si_3$, octamethyltrisiloxane) for vapor expansion in the close proximity of the liquid-vapor saturation curve, at relatively low pressure of operation. A supersonic flow is attained within the divergent section of the nozzle, as demonstrated by the observation of an oblique shock wave at the throat section, where a 0.1 mm recessed step is located. Schlieren visualizations are limited by the occurrence of condensation along the mirror side of the nozzle. Pressure measurements are compatible with the observed flow field.

## 1. INTRODUCTION

Organic Rankine Cycle (ORC) is a well established and viable technology for the exploitation of energy from low/medium temperature sources, such as renewable or heat-recovery, with applications to low/medium electrical power generation and Combined Heat and Power (CHP) plants. For these applications, the ORC technology is usually preferred over steam cycle due to the simplicity of plant components, high reliability and low operational costs Gaia and Duvia (2002); Bini and Manciana (1996) and relatively high efficiency of the thermodynamic cycle Angelino et al. (1984).

Turbine efficiency in current ORC plants is around 75-85%, see Schuster et al. (2009); Duvia and Tavolo (2008) and recent researches in ORC technology are focused on blade geometry optimization to improve the turbine efficiency. This task is complicated by the fact that the use of organic compounds operating close to the vapor saturation curve in ORC results in highly

non-ideal compressible-fluid flows within the turbine passages, which are usually designed to operate in supersonic flow conditions due to the relatively low speed of sound which characterizes high molecular mass fluids, especially in close-to-saturation flow conditions Harinck et al. (2009). Moreover, the accurate prediction of the flow behavior requires the use of complex non-ideal thermodynamic models. Computational Fluid Dynamics (CFD) codes for non-ideal compressible-fluid dynamics (NICFD) are already available which implement the complex thermodynamics of fluids in ORC turbine passages Colonna and Rebay (2004); Guardone (2007); Cinnella and Congedo (2007); Colonna et al. (2008); Hoffren et al. (2002).

Currently, no experimental data of non-ideal compressible-fluid flows are available to support our understanding of the fluid dynamics of ORC plants and to assess the reliability and accuracy of available thermodynamics models and CFD tools.

To investigate experimentally the non-ideal compressible-fluid flows of organic compounds in typical operating conditions for ORC applications, the *Test Rig for Organic Vapors* (TROVA) was designed and constructed at the Politecnico di Milano, see Spinelli et al. (2013). In the facility, expansion flows of different organic compounds in non-ideal conditions in the close proximity of the liquid-vapor saturation curve can be investigated by independent measurements of pressure, temperature and velocity. The facility implements an ORC (either sub-critical or super-critical), where the expansion process take place within a nozzle replacing the turbine. A straight axis converging-diverging nozzle was chosen, being it the simplest geometry providing an expansion from subsonic to supersonic flow in the operating conditions of interest. The size of the nozzle is large enough to guarantee that within the expanding flow a large isentropic core is preserved, thus making it possible to measure temperature and pressure fields without the use of calibrated probes, see Spinelli et al. (2010). Total pressure and temperature are measured in the settling chamber ahead of the nozzle inlet; static pressure taps at different sections along the nozzle axis are used to follow the flow evolution as it expands from rest to supersonic conditions. In order to reduce the required input thermal power, a batch operating facility has been selected.

The structure of the paper is as follows. In section 2, the general set-up of the test-rig is presented and an overview of the measurement techniques is given. In section 3, experimental results with air are reported. In particular, the operation of the throttling valve is verified and the complete measurement system is tested. The possibility of using the Schlieren visualization to support the interpretation of the pressure measurement is assessed. In section 4, preliminary experimental results for siloxane fluid MDM ($C_8H_{24}O_2Si_3$, octamethyltrisiloxane) are reported. In particular, the heating and degassing procedure is tested and assessed against saturated data for MDM fluid. A very preliminary test run at low pressure (in the range 70-350 mbar) is described and the suitability of the set-up to investigate nozzle flows of non-ideal compressible flows of organic fluids is discussed. Final remarks and observations are gathered in section 5.

## 2. TROVA: SET-UP AND MEASUREMENT TECHNIQUES

The TROVA operates as a blow-down wind tunnel, namely, in a discontinuous way, to reduce the power requirements. The working fluid to be tested is stored in a high pressure vessel (HPV) (see figure 1) and isochorically heated up to saturated, superheated, or supercritical conditions (point 4 in figure 1) at a pressure $P_4$ and temperature $T_4$ above the nozzle stagnation conditions (point 6). The heating elements consist of electrical bands and wires externally clung to the vessel. The control valve (MCV) regulates the feeding total pressure $P_{T6}$ at the inlet of the nozzle during the entire test. Small fluctuations in pressure around the set-point are acceptable since they are characterized by a time scale extremely large if compared to the nozzle characteristic

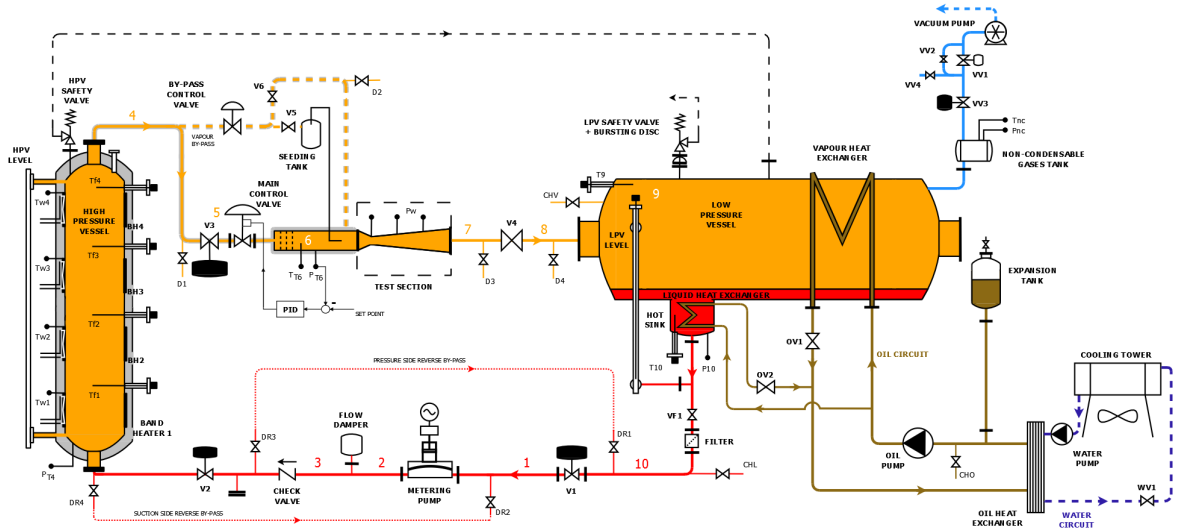


**Figure 1: Scheme of the TROVA test-rig. The total pressure and temperature in the settling chamber are measured by sensors $P_{T6}$ and $T_{T6}$, respectively. Static pressure taps in the test section are indicated by $P_w$.**

| Fluid | $P_{T6}$ (bar) | $T_{T6}$ (°C) | $Z_{T6}$ | $\beta$ | $P_7$ (bar) | $M_7$ | $t$ (s) |
|---|---|---|---|---|---|---|---|
| MDM | 4.0 | 253.2 | 0.85 | 10.0 | 0.4 | 2.05 | $\sim 40$ |

**Table 1: Operating conditions for the first MDM test and expected duration. The expansion ratio $\beta$, exit pressure $P_7$ and exit Mach number $M_7$ refer to adapted conditions.**

time. Similarly, the reduction of the nozzle inlet total temperature $T_{T6}$ due to the HPV emptying process is small, thanks to the high molecular complexity of the working fluid, i.e., large heat capacity, and occurs at a very small time rate. However, in the settling chamber ahead of the nozzle, the stagnation conditions data $P_{T6}$ and $T_{T6}$ are acquired at frequency of orders of magnitude higher with respect to the frequency content of each signal. The organic vapor is then expanded (to state 7) through the nozzle, where wall pressure measurements are performed. The vapor is discharged into a large area pipe (point 8), where it is slowed and brought in a low pressure vessel (LPV, state 9) where the fluid is collected and condensed (state 1). The loop is closed by the liquid compression to the HPV (point 2), performed by a membrane metering pump. Further details concerning all components can be found in Spinelli et al. (2013).

The design test scheduled for the TROVA concerns the expansion flow of siloxane MDM. Due to its relatively high critical temperature ($T_C = 290.94$ °C), its thermal stability, non-toxicity and low cost, this fluid is of particular interest for industrial ORC plant exploiting relatively high temperature sources (e.g. biomass, solar radiation). The operating conditions for this test have been selected as a compromise between the requirement of moderate temperatures, in order to avoid fluid decomposition during the early tests, and the need of expanding the vapor through thermodynamic regions where non-ideal compressible-fluid effects are appreciable. The resulting conditions are reported in table 1.

### 2.1 Test section and instrumentation

The test section is made of a planar converging-diverging nozzle (see figure 2); the diverging portion of the nozzle profile was designed by applying the method of characteristics coupled with state-of-the-art thermodynamic models for the siloxane MDM (Guardone et al. (2013),Colonna

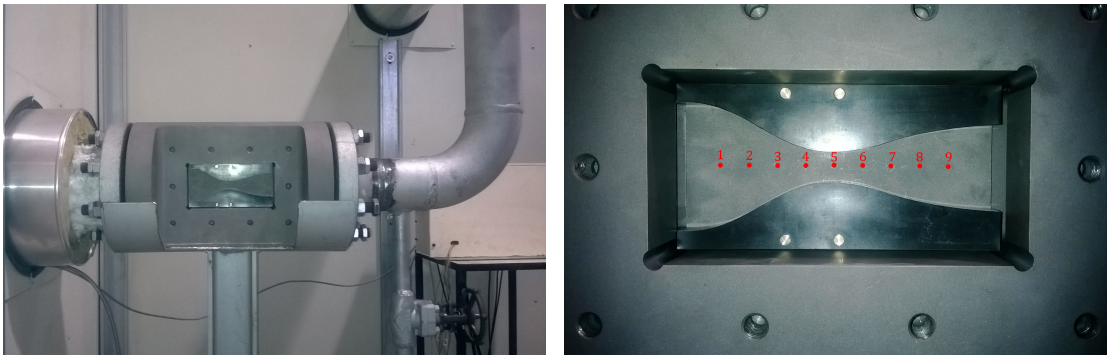


(a) (b)

**Figure 2: Overview of the test section (a) and details of the nozzle within the test section (b). The flow is from left to right. The settling chamber is on the left and it is enclosed in the white box which contains the TROVA and it is separated from the laboratory for safety. The front window is made of quartz to allow for optical access, the back closure is a mirror (not installed to take the picture). Static pressure taps are located along the symmetry axis and are marked with red dots.**

| **Property** | **Sensor** | **Type** | **CR *P*** (**bar**) | **CR *T*** (**°C**) | **U$_2$ *P*** (**%FS**) | **U$_2$ *T*** (**°C**) |
|---|---|---|---|---|---|---|
| $T_T$ | Thermocouple | J (Fe - Cu/Ni) | - | 25-250 | - | 0.4 |
| $P_T$, $P_w$ | Piezo-resistive | Kulite XTEH | 1-FS (3.5-40) | 25-250 | 0.07 | - |

**Table 2: Type, calibration range (CR) and expanded uncertainty (U$_2$) of the instruments employed for pressure and temperature measurements. FS is the transducer full scale.**

et al. (2006)), while the converging portion was represented by a $5^{th}$ order polynomial profile which realizes a smooth transition from the inlet to the throat section. At the geometrical throat a recessed step of 0.1 mm depth (1.2% of the nozzle semi-height at the throat) was machined on both the top and bottom contoured profiles, in order to fix the location of the minimum nozzle area, independently from boundary layer unsteadiness.

The front planar wall is a quartz window which guarantees optical access, while the rear wall is made by a steel plate and it houses 9 pressure taps along the nozzle axis. Behind each tap a 25 mm long pneumatic line-cavity system is machined in the plate body, connecting the tap with the sensing element of a piezo-resistive pressure transducer. For the present experimentation, the plate surface has been mirror polished, in order to allow the implementation of the double-passage Schlieren visualization technique detailed in section 2.2. The stagnation conditions are measured in the settling chamber ahead of the test section. A wall pressure tap/line/transducer system (similar to the nozzle ones) is used for the total pressure, due to the very low flow velocity in the chamber; the total temperature is measured by a J type thermocouple whose hot junction is located at the chamber axis.

The pneumatic lines connecting each pressure measurement point with the corresponding transducer are characterized by very short length ($\sim$ 25 mm) and small diameter ducts (0.3 to 1.5 mm); similarly the volume of the capacities ahead of the transducer sensing element is extremely small ($\sim$ 45 $mm^3$). A natural frequency of about 900 Hz has been estimated for the transmission lines. All pressure sensors are piezo-resistive transducers (Kulite XTEH-7L series) operating at high temperature (up to 343 °C) and chemically compatible with almost all working fluids of interest for the ORC industry. The data acquisition (DAQ) system consist

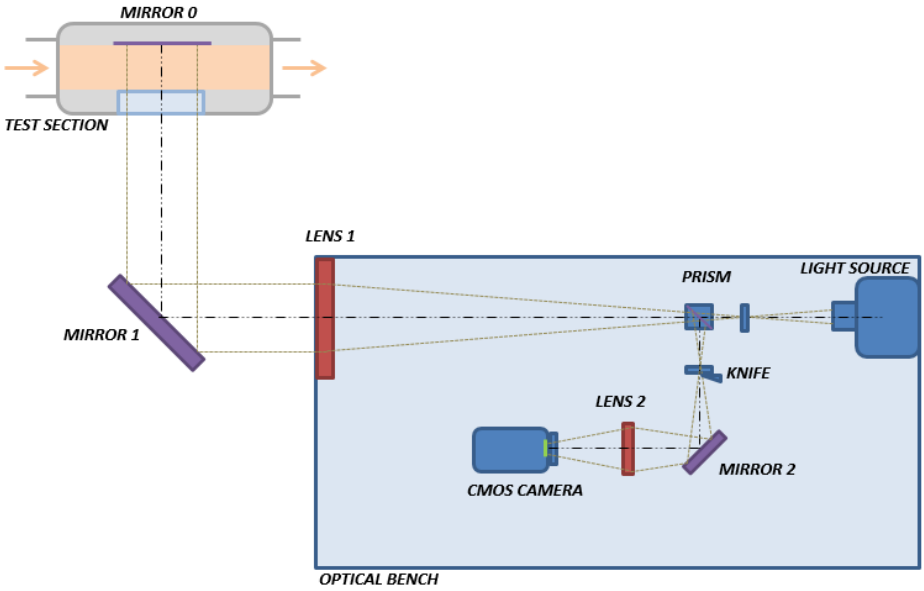


**Figure 3: Functioning scheme of the double-passage Schlieren set-up.**

of analog modules employed to provide the voltage supply to the transducers and to amplify the measurement signals (including the thermocouple output voltage) and of a high speed data acquisition board.

The J thermocouple has been calibrated in the temperature range 25-250 °C. Due to the large sensitivity of the pressure transducers to temperature variation and the consequent uncertainty increase, the pressure sensors were calibrated both in pressure and in temperature in the range 1-FS bar for the pressure and 25-250 °C for the temperature. The final accuracy, expressed in terms of expanded uncertainty, obtained for each sensor is summarized in table 2. Notice that the acquisition channels and the supply/amplification modules are kept unchanged during both the calibration and the measurement processes.

### 2.2 Schlieren set-up

A double pass-type parallel light Schlieren system with the emitting and receiving optical components mounted on an optical table was used. This configuration is shorter and easier to align with respect to the classical Z-type system. A schematic sketch of the system is shown in figure 3. A 100 W Hg arc-lamp is used as the light source. The light from the lamp is focused by a F/1.5 silica lens into a circular spot of about 3 mm in diameter and then collimated to form parallel light rays by a Schlieren lens head (Lens 1 in figure 3). The latter has a diameter of 150 mm and a focal length of 1000 mm. The collimated light beam is deflected by a circular mirror (Mirror 1 in figure 3) before traversing the test section. It is then reflected back to the Schlieren head by the metallic mirror 0 (namely, by the polished nozzle back wall) and focused on the vertically aligned knife edge (knife in figure 3)). The knife orientation allows to visualize the density gradient along the nozzle axis. A cubic beamsplitter (prism in figure 3) separate the light beam originated by the light source and the reflected one. A lens of 160 mm focal lenght and 50 mm diameter is located behind the knife (Lens 2 in figure 3) and forms a real image of the test section on the sensor of a high speed CMOS camera. To allow a suitable long recording time the CMOS camera resolution and frame rate were respectively set to 1024 x 512 pixels and to 100 fps (frames per second), while the exposure time was set to 20 $\mu$s.

| **Fluid** | $P_{T6}$ (**bar**) | $T_{T6}$ (**°C**) | $Z_{T6}$ | $\beta$ | $P_7$ (**bar**) | $M_7$ | $t$ (**s**) |
|---|---|---|---|---|---|---|---|
| Air | 4.0 | 20-60 | 1.0 | 20.0 | 0.2 | 2.59 | $\sim 40$ |

**Table 3: Operating conditions for the air test and expected duration. The expansion ratio $\beta$, exit pressure $P_7$ and exit Mach number $M_7$ refer to adapted conditions.**

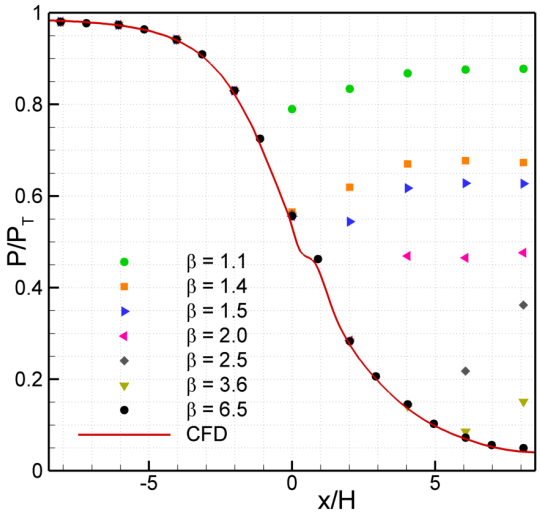


**Figure 4: Pressure measurement along the nozzle axis for different values of the expansion ratio $\beta$. Pressure is made non-dimensional by the upstream total pressure $P_T$. The throat is located at $x/H = 0$. H is the nozzle semi-height at the throat.**

## 3. EXPERIMENTAL RESULTS WITH AIR

### 3.1 Equivalent test with air

In order to verify the suitability of the test procedure and of the measuring strategy in giving reliable measurements and an accurate description the nozzle flow field, an equivalent test is designed and performed using dry air as working fluid. This allows for a comparison with theory based on the ideal gas model, with similar experiments in nozzle (available from the literature), and with standard CFD simulations. The equivalent test was designed in order to have a comparable duration with respect to the MDM 1st test (see table 1), thus a similar dynamic operation of the plant. Therefore, the capability of the control valve MCV in keeping a reasonably constant pressure at the nozzle inlet during the test can be verified. The converging-diverging nozzle profile designed for the MDM 1st test was used. However, when operated with air, the nozzle adapted expansion ratio and exit Mach number considerably differ from the corresponding design values for MDM expansion. The operating conditions of the equivalent test are summarized in table 3.

The air tests were performed by storing in the HPV air at a pressure of about $P_{T4} = 12$ bar and at a temperature in the range $T_{T4} =$ 20-160 °C. The LPV pressure is brought to $P_{T9} = 0.08$ bar by evacuating the reservoir. Therefore, at the initial time ($P_7$=$P_{T9}$) the nozzle is under-expanded, since the expansion ratio is $\beta = P_{T6}/P_7 = 50$. The test start is dictated by the opening of the ball valve V3 (see figure 1) which also triggers the CMOS camera recording, in such a way that the pressure and temperature data are synchronized with the Schlieren images. The control valve operates with low frequency oscillations (of the order of 1 Hz) keeping the nozzle inlet total pressure at a value of about $P_{T6} = 4 \pm 0.1$ bar for approximately 25 s, than the MCV is fully opened and the pressure across the valve is balanced ($P_{T4}$=$P_{T6}$). The test

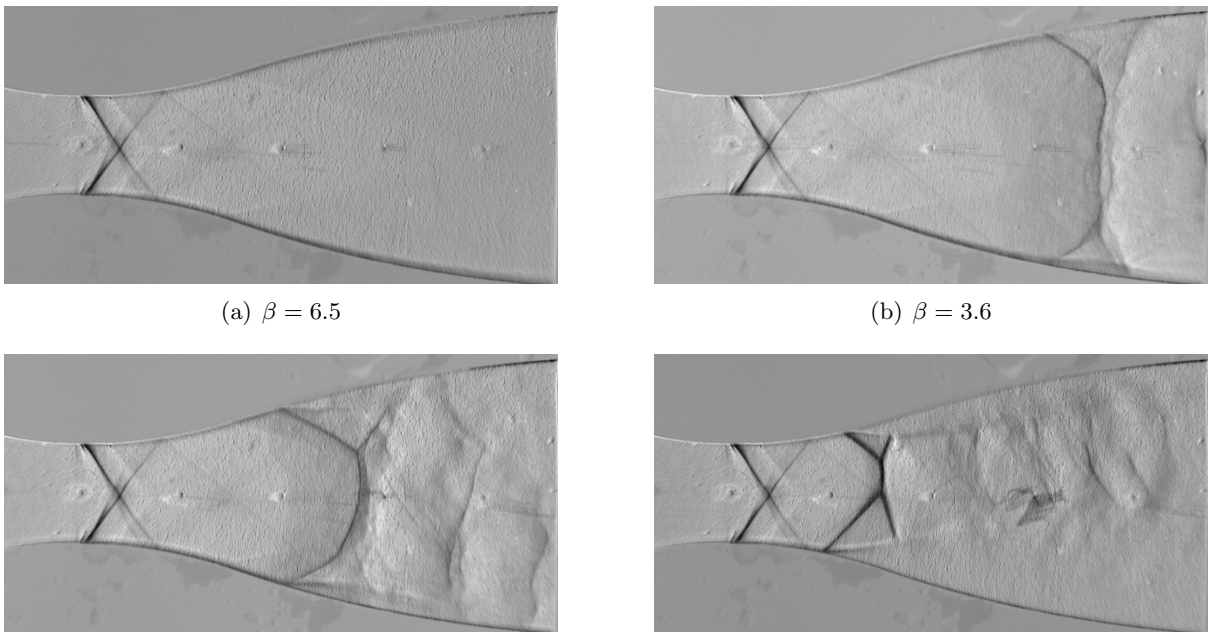

(a) $\beta = 6.5$ (b) $\beta = 3.6$

(c) $\beta = 2.5$ (d) $\beta = 2$

**Figure 5: Schlieren visualization of nozzle operation in air in chocked conditions for four values of the expansion ratio $\beta$, corresponding to adapted conditions (a) and subsonic outflow with a shock wave in the divergent section (b,c,d). A recessed step 0.1 mm deep is machined at the throat section of geometry shown on top: a fan-shock-fan system originates at the step location. Pressure measurements are reported in figure 4.**

proceeds for additional 15 s (with a reducing and uncontrolled $P_{T6}$) until the pressure of the two reservoirs are balanced ($P_{T4}$=$P_{T9}$) (due to the HPV emptying and the LPV filling). According to this test scheme, the entire range of possible flow regimes in the nozzle are observed during the test: from under-expanded/adapted/over-expanded to fully subsonic flow.

### 3.2 Test results

The values of the static to total pressure ratio are reported in figure 4 for all static pressure taps along the nozzle axis and for different values of the expansion ratio $\beta$. Note that pressure taps along the back plate are not symmetric and up to 17 different measurement station can be obtained if different tests are carried out by changing the plate orientation. Numerical simulations of the expansion process, including the geometry of the recessed step, agree fairly well with the adapted flow conditions within the nozzle ($\beta = 6.5$) in figure 4. Note that the isentropic expansion profile is perturbed by the presence of the recessed step at the nozzle throat, as confirmed by the numerical simulations as well as by the experimental results. At lower values of $\beta$, the measured pressure profiles departs from the adapted one, as expected from the gasdynamic theory of nozzle flows.

Indeed, as confirmed also by the Schlieren measurements in figure 5, shock waves occurs in the divergent portion of the nozzle for low enough expansion ratios. For $\beta = 1.1$ and $\beta = 1.4$ (see figure 4) a fully subsonic flow is observed in both the convergent and the divergent section of the flow; notice that in case of $\beta = 1.4$ sonic conditions are reached at throat. Remarkably, the recessed step at the nozzle throat produces significant perturbation in the flow field, which are clearly visible in all Schlieren visualizations in figure 5 and in the pressure profiles in figure 4. Supersonic flow expansion at the step location results in the formation of a Prandtl-Meyer fan

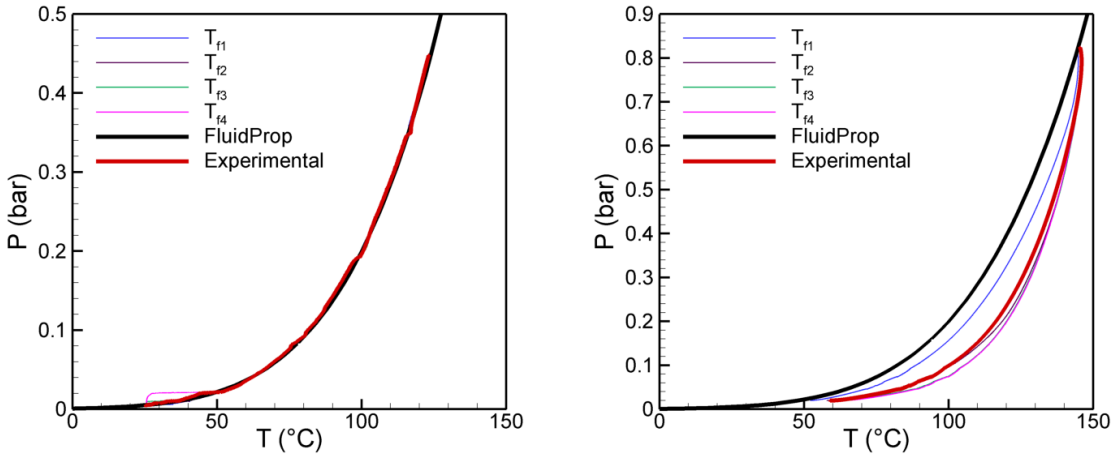


(a) Heating phase

(b) Cooling

**Figure 6: Pressure-temperature profile during the heating (a) and cooling (b) phase and saturation curve of fluid MDM.**

(light gray in the Schlieren images) and causes flow separation around the step corner. Flow re-attachment at the nozzle surface results in the formation of a shock wave (dark gray). A further expansion is visible at the geometric discontinuity at the end of the machined portion of the nozzle. The resulting fan-shock-fan combination is clearly seen to propagate and to interact with the nozzle walls in the adapted flow conditions shown in 5a).

## 4. PRELIMINARY RESULTS FOR MDM VAPOR

### 4.1 Fluid preparation and heating/cooling procedure

The preliminary steps required to prepare the MDM test include the fluid charge and the execution of cycles of isochoric heating and cooling within the HPV for removing incondensable gases, most notably air, from the fluid. The fluid was charged at the condenser (LPV) after a complete plant evacuation, which was carried out using the plant vacuum pump. The final pressure before the charge (at each section) was of the order of 1 mbar. Depending on the test conditions a proper fraction of the liquid is pumped to the HPV by the metering pump, whose operation was also verified. The mass of fluid charged at each section is such that, at room temperature, the fluid is always in saturated conditions, therefore at a pressure well below the atmospheric pressure.

The heating/cooling cycles were performed from room temperature ($\sim$ 20℃) to about 180 ℃, therefore below the critical point and always maintaining saturated conditions, namely by keeping the fluid within the two-phase region. It's worth reminding that the HPV is electrically heated from the vessel external walls and it is not equipped with a cooling system, therefore cooling can be obtained only by heat exchange with the external environment.

Figure 6 shows that the experimental $P$-$T$ saturation curve obtained during the heating process is finely captured by the thermodynamic model Colonna et al. (2006), whereas the agreement is lost during the cooling process. Indeed, during the heating process the convective heat transfer between the fluid and the thermocouple (industrial K type) hot junctions (located at the reservoir axis) is promoted by the expected convective motion within the reservoir (activated by the liquid boiling in the lower portion of the reservoir, where most of the thermal energy enters the system). This heat transfer mechanism is expected to prevail over the conduction

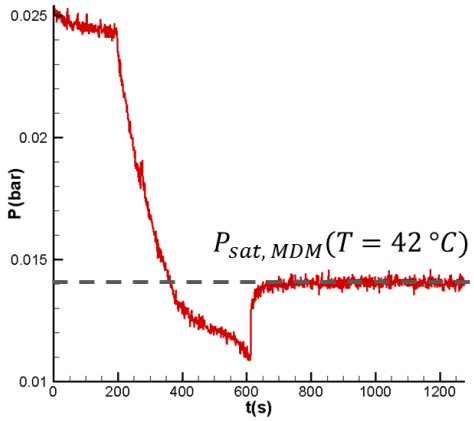


**Figure 7: Pressure in the HPV during the degassing cycle at a temperature of 42 °C.**

| **Fluid** | $\boldsymbol{P_{T6}}$ **(bar)** | $\boldsymbol{T_{T6}}$ **(°C)** | $\boldsymbol{Z_{T6}}$ | $\beta$ |
|---|---|---|---|---|
| MDM | 0.35-0.07 | 120-80 | 0.97 | 50-10 |

**Table 4: Operating conditions for the early MDM tests.**

along the thermocouple stem and the radiation from the vessel wall. During the cooling process, convective motions are strongly inhibited, since the the entire HPV (and especially its top portion) is not provided with a cooling system and it is strongly insulated. Therefore, the thermocouple are presumably heated by conduction and radiation from the vessel wall at a temperature constantly higher than the condensing fluid temperature.

After each heating/cooling cycle, the HPV pressure is significantly higher than the saturation pressure at the fluid temperature (see figure 7, at $t < 200$ s). This could be related to the presence of air sucked by HPV from the surrounding environment, to liquid degassing or to fluid decomposition, since MDM is expected to form more volatile fractions after decomposition. For this reason, after each cycle the HPV has been degassed, by means of the vacuum pump. The process is depicted in figure 7. It can be seen that as the vacuum pumps is operating (staring at $t \simeq 200$ s) the HPV pressure reduces at a large rate (until $t \simeq 400$ s) this behaviour is probably related to volatile gas extraction (air, non-condensible gas, possible decomposition products). As the pressure diminishes the rate of decrease also reduces, indicating the approaching of the saturation pressure and the consequent probable extraction of MDM vapor. As the vacuum pump is stopped (at $t \simeq 600$ s), the pressure rapidly rise, reaching and keeping constant the saturation value, thus indicating that no fluid decomposition occurred. This matching is also a confirmation of the consistency between the experimental and the calculated P-T value at this saturation point ($P = 0.014$ bar, $T = 42$ °C).

### 4.2 Experimental results

Due to the difficulties related to the accurate setting of the MCV PID parameters, the early test with MDM are performed with a constant valve opening set at 25%. The resulting test conditions are reported in table 4.

A picture of the test section during the experimental runs with MDM is shown in figure 10. Condensation of MDM vapor occurred along the back plate, which is not heated, in all performed tests. Condensation prevented the use of the double-passage Schlieren techniques, since liquid

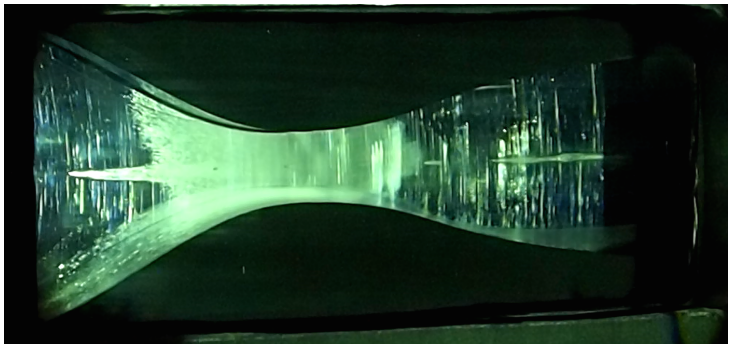

**Figure 8: Picture of the test section during the experimental runs with MDM. The flow is from left to right. Condensation along the back plate is clearly visible. A liquid film is also visible in the convergent section of the nozzle.**

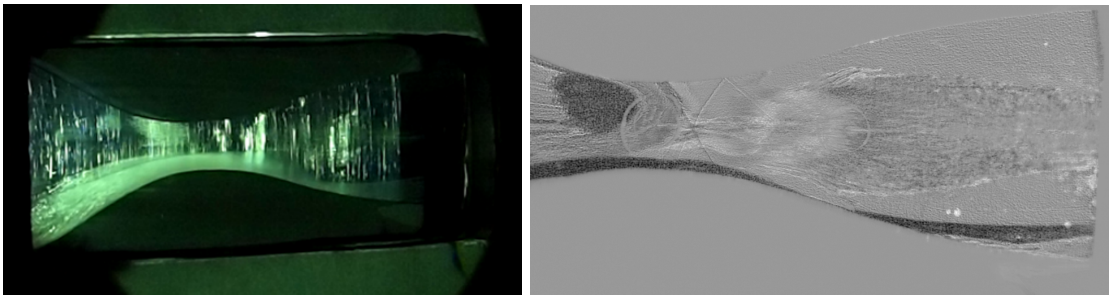

(a) (b)

**Figure 9: Last part of the experimental run with MDM. The flow is from left to right. Total inlet conditions at this time are $P_{T6} = 100$ mbar, $T_{T6} = 84$ °C; the downstream pressure is $P_9 = 6$ mbar. (a) Picture of the test section; the liquid film is largely evaporated at the back plate. (b) Schlieren visualization; oblique shock waves immediately downstream of the recessed step are clearly visible.**

drops and film over the back plate produced reflected rays featuring highly distortion in different directions, thus preventing the detection of the density gradients in the vapor phase. Direct observation of the test section revealed that indeed condensation occurs only along the metal plate. Moreover, two shock waves originating from step position were observed thus confirming the possibility of observing a supersonic nozzle flow in the vapor phase. This is also proved by partial Schlieren visualization of figure 9 obtained during the last part of the test, when the test section heating provided by the vapor flow is such that the liquid film is largely evaporated. The oblique shock waves originated immediately after the recessed step are clearly visible (together with their reflection at the contoured wall), thus confirming the occurrence of a supersonic flow of MDM vapor within the nozzle.

Figure 10 reports the instantaneous Mach number at the pressure tap located along the nozzle axis and at the throat section. The Mach number is computed from isentropic relations using the instantaneous values of the total and static pressure ratio and according to the pertinent thermodynamic model. From small-perturbation theory of transonic flows, the value of the Mach number in this peculiar location is independent from the fluid thermodynamics. Therefore the ideal-gas value measured for air (about 0.96) should be equal to that obtained for MDM in non-ideal conditions. Indeed a good agreement is observed during the first 15 s of the experiment, thus confirming the consistency of the pressure measurements. Departure from the expected value is believed to be related also to the presence of a thick liquid film along the bottom surface of the nozzle, probably caused by liquid entrainment within the main vapor flow from

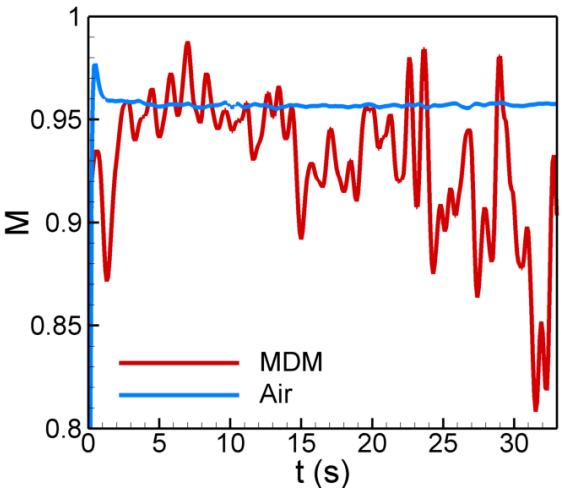


**Figure 10: Mach number from the pressure tap located along the nozzle axis and at the throat section for the air and MDM test runs.**

the settling chamber.

## 5. CONCLUSIONS

Preliminary results from the Test-Rig for Organic Vapors (TROVA) at Politecnico di Milano were reported. Pressure measurements are in good agreement with theoretical predictions for air, thus confirming the accuracy of the measurement chain and the efficiency of the throttling valve. The Schlieren bench is functional and provides an overview of the flow field, including the location of shock waves which is required to understand the pressure signal in the diverse operating conditions. Regarding the test run with the organic fluid MDM, the loading procedure and the liquid pump operation was verified. Degassing of the fluid is satisfactory: after vacuumising the HPV, the pressure immediately sets back to the vapor pressure at the considered temperature. The fluid follows the saturation curve while heating, thus indicating that no contaminants are present. Preliminary results for nozzle flow of MDM were found to be consistent with those obtained for air, though condensation along the back plate prevented its use as a mirror for the optical measurements. The appearance of shock waves induced by the recessed step confirms the occurrence of a supersonic nozzle flow of MDM in the vapor phase, during the last part of the test. The test-rig is currently being retrofitted with a new heating system to avoid condensation during the fluid heating phase, most notably in the piping connecting the HPV and the test section, and during the test runs.

## REFERENCES

Angelino, G., Gaia, M., and Macchi, E. (1984). A review of italian activity in the field of organic rankine cycles. In *VDI Berichte - Proceedings of the International VDI Seminar, Zrich*, volume 539, Dsseldorf. VDI Verlag.

Bini, R. and Manciana, E. (1996). Organic rankine cycle turbogenerators for combined heat and power production from biomass. In *Energy Conversion from Biomass Fuels, Current Trends and Future System, Munich.*

Cinnella, P. and Congedo, P. M. (2007). Inviscid and viscous aerodynamics of dense gases. *J. Fluid Mech.*, 580:179–217.

Colonna, P., Harinck, J., Rebay, S., and Guardone, A. (2008). Real-gas effects in organic rankine cycle turbine nozzles. *J. Prop. Power*, 24:282–294.

Colonna, P., Nannan, R., Guardone, A., and Lemmon, E. W. (2006). Multi-parameter equations of state for selected siloxanes. *Fluid Phase Equilib.*, 244:193–211.

Colonna, P. and Rebay, S. (2004). Numerical simulation of dense gas flows on unstructured grids with an implicit high resolution upwind Euler solver. *Int. J. Numer. Meth. Fluids*, 46(7):735–765.

Duvia, A. and Tavolo, S. (2008). Application of orc units in the pellet production field: technical-economic considerations and overview of the operational results of an orc plant in the industry installed in madau (germany). Technical report, Turboden s.r.l., Italy.

Gaia, M. and Duvia, A. (2002). Orc plants for power production from biomass, 0.4-1.5 MWe: technology, efficiency, practical experiences and economy. In *7th Holzenergie Synposium*. ETH Zurich.

Guardone, A. (2007). Three-dimensional shock tube flows of dense gases. *J. Fluid Mech.*, 583:423–442.

Guardone, A., Spinelli, A., and Dossena, V. (2013). Influence of molecular complexity on nozzle design for an organic vapor wind tunnel. *ASME Journal of Engineering for Gas Turbines and Power*, 135:042307.

Harinck, J., Guardone, A., and Colonna, P. (2009). The influence of molecular complexity on expanding flows of ideal and dense gases. *Phys. of Fluids*, 21:086101, 1–14.

Hoffren, J., Talonpoika, T., Larjola, J., and Siikonen, T. (2002). Numerical simulation of real-gas flow in a supersonic turbine nozzle ring. *J. Eng. Gas Turbine Power*, 124:395–403.

Schuster, A., Karellas, S., Kakaras, E., and Spliethoff, H. (June 2009). Energetic and economic investigation of organic rankine cycle applications. *Applied Thermal Engineering*, 29(8-9):1809–1817.

Spinelli, A., Dossena, V., Gaetani, P., Osnaghi, C., and Colombo, D. (2010). Design of a test rig for organic vapours. In *Proceedings of ASME Turbo Expo, Glasgow, UK*.

Spinelli, A., Pini, M., Dossena, V., Gaetani, P., and Casella, F. (2013). Design, simulation, and construction of a test rig for organic vapours. *ASME Journal of Engineering for Gas Turbines and Power*, 135:042303.

## ACKNOWLEDGEMENT

The research is funded by the European Research Council under Grant ERC Consolidator 2013, project NSHOCK 617603. The initial layout of the plant was funded by Turboden S.r.l..